Comput Geosci (2010) 14:451–464
DOI 10.1007/s10596-009-9163-9

ORIGINAL PAPER

A global approach to reactive transport: application to the MoMas benchmark

Caroline de Dieuleveult · Jocelyne Erhel

Received: 14 August 2008 / Accepted: 3 September 2009 / Published online: 2 October 2009

Abstract Water resource management involves numerical simulations in order to study contamination of groundwater by chemical species. Not only do the aqueous components move due to physical advection and dispersion processes, but they also react together and with fixed components. Therefore, the mass balance couples transport and chemistry, and reactive transport models are partial differential equations coupled with nonlinear algebraic equations. In this paper, we present a global method based on the method of lines and differential algebraic system (DAE) solvers. At each time step, nonlinear systems are solved by a Newton-LU method. We use this method to carry out numerical simulations for the reactive transport benchmark proposed by the MoMas research group. Although we study only 1D computations with a specific geochemical system, several difficulties arise. Numerical experiments show that our method can solve quite difficult problems, get accurate results and capture sharp fronts.

This work was partly supported by a grant from ANDRA (National Radioactive Waste Management Agency) and by a grant from the GdR MoMas (part of the French PACEN program).

C. de Dieuleveult
ANDRA and INRIA-Rennes, Campus de Beaulieu, Rennes, France
e-mail: caroline.de_dieuleveult@mines-paristech.fr

J. Erhel (✉)
INRIA-Rennes, Campus de Beaulieu, Rennes, France
e-mail: jocelyne.erhel@inria.fr

Keywords Reactive transport · Geochemical modelling · Method of lines · Differential algebraic equations · Newton method · Sparse LU factorisation

Mathematics Subject Classifications (2000)
MSC 65N40 · MSC 65L80

1 Introduction

The behaviour of potential storage sites is governed by many complex physico-chemical mechanisms. Numerical simulations are carried out in order to contribute to safety evaluations and risk assessment. In this paper, we focus on chemistry as well as transport of the aqueous solutions. In order to take into account these two phenomena simultaneously, we need to consider a coupled model.

Two types of methods have been described in the literature for carrying out simulations for this reactive transport model. The sequential approaches [3, 20, 26, 28, 30, 32] separately solve the equations while global approaches [13, 23, 26, 27] simultaneously solve the whole system. Whereas the first approach involves the consecutive solutions of decoupled systems and allows the use of methods adapted to each model, it requires, in general, very small time steps. Because of high memory requirements, the global approach was first rejected [29], but the memory capacity of computers has greatly improved so that a high memory requirement is no longer a crucial drawback. Moreover, a global approach requires generally fewer iterations than a sequential iterative approach and may allow larger time steps. Thus, a global approach is sometimes preferable [6, 25, 26].

In this paper, we present a global approach based on a framework of partial differential algebraic equations (PDAEs). We consider a geochemical model composed of homogeneous and heterogeneous reactions at equilibrium. We could also consider kinetic reactions, with a slight modification of our method. Concerning transport, we assume that the velocity and the diffusion tensor are independent of species and that porosity is independent of the time variable. Because of this assumption, the transport operator is linear, and we can rewrite the transport equations by introducing total variables. We assume that the coupled problem is well-posed.

The method is described in detail in [11, 12]. Here, we present results obtained for the MoMas benchmark [5]. The main objective of this benchmark is to check numerical methods against numerical complexity. We study the so-called 1D easy test case, where hydrodynamics and chemistry are simplified. The 1D computational domain is composed of two media, there are neither kinetic nor precipitation–dissolution reactions. On the other hand, numerical difficulties are artificially increased. Our main objective is to get accurate results. Therefore, we use a fine mesh and small tolerances in our simulations. We check convergence in our numerical experiments and focus on specific behaviour such as numerical oscillations. This benchmark is also studied by other participants [4, 16, 19, 22]. Our results are in good agreement with theirs. The paper is organised as follows: Section 2 presents the mathematical model based on total concentrations and on a coupled PDAE system. Then, in Section 3, we describe the numerical model based on the method of lines and a coupled discrete DAE system. Finally, Section 4 presents the results obtained with the 1D easy test case of the MoMas benchmark.

2 Mathematical model

We consider a groundwater chemical system containing N_e species, which interact due to chemical reactions. In addition, the mobile species are transported by advection and dispersion. The mathematical model is thus composed of chemistry equations coupled to transport equations.

2.1 Chemistry equations

For the geochemical system considered, we assume a thermodynamic equilibrium at any time. Aqueous and sorption reactions can be expressed in terms of nonlinear algebraic equations based on mass action laws. Some species, named secondary species, can be expressed as functions of others, referred to as components [21, 29]. In fact, components form the minimum set of species required in the model. We make a distinction between aqueous species and fixed species. For the sake of simplicity, we assume here that all activity coefficients of the aqueous and fixed species are equal to 1, so that the species can be identified with their concentration. Thus, the mass action laws can be written

$$\begin{cases} u_i(x,t) = K_i^u \displaystyle\prod_{j=1}^{n_c} c_j(x,t)^{S_{ij}}, & i = 1, \ldots n_u, \\ v_i(x,t) = K_i^v \displaystyle\prod_{j=1}^{n_c} c_j(x,t)^{A_{ij}} \prod_{k=1}^{n_s} s_k(x,t)^{B_{ik}}, & i = 1, \ldots n_v, \end{cases} \tag{1}$$

where c_j, $j = 1, \ldots n_c$ and s_k, $k = 1, \ldots n_s$ are, respectively, the concentrations of the n_c aqueous and n_s fixed components, whereas u_i, $i = 1, \ldots n_u$ and v_i, $i = 1, \ldots n_v$ are, respectively, the concentrations of the n_u aqueous and n_v fixed secondary species. The matrices $\mathbf{S} \in \mathbb{R}^{n_u \times n_c}$, $\mathbf{A} \in \mathbb{R}^{n_v \times n_c}$ and $\mathbf{B} \in \mathbb{R}^{n_v \times n_c}$ contain the stoichiometric coefficients, and the vectors $\mathbf{K}^u \in \mathbb{R}^{n_u}$ and $\mathbf{K}^v \in \mathbb{R}^{n_v}$ contain the equilibrium constants. By definition of components and secondary species, the matrix $\begin{pmatrix} \mathbf{S} & \mathbf{0} \\ \mathbf{A} & \mathbf{B} \end{pmatrix}$ is of full rank.

Precipitation–dissolution reactions are governed by different laws from aqueous and sorption reactions. Again, we assume that the activity of a precipitated species is equal to one, and we identify a precipitated species by its number of moles per unit of volume p_i. In the general case, precipitated species do not exist at any time; thus, their fraction can be zero. This general model involves nonsmooth nonlinear equations and can be written as a complementary problem. Here, we assume that the number of precipitated species n_p is known and constant in time. With this restriction, precipitation–dissolution laws are differentiable and can be written

$$\begin{cases} p_i \geq 0, & i = 1, \ldots n_p, \\ 1 = K_i^p \displaystyle\prod_{j=1}^{n_c} c_j(x,t)^{E_{ij}}, & i = 1, \ldots n_p. \end{cases} \tag{2}$$

As previously, $\mathbf{E} \in \mathbb{R}^{n_p \times n_c}$ is the matrix of stoichiometric coefficients and $\mathbf{K}^p \in \mathbb{R}^{n_p}$ is the vector of equilibrium constants related to precipitation.

We rewrite the previous laws in a logarithmic form. Indeed, all concentrations must have positive values. This chemical constraint is guaranteed by using logarithms. With $\ln(\mathbf{c}), \ln(\mathbf{s})$ and $\mathbf{p}$ as primary unknowns, the new chemical model is given by

$$\begin{cases} \mathbf{u}(x,t) = \exp(\ln(\mathbf{K}^u) + \mathbf{S}\ \ln(\mathbf{c}(x,t))), \\ \mathbf{v}(x,t) = \exp(\ln(\mathbf{K}^v) + \mathbf{A}\ \ln(\mathbf{c}(x,t)) + \mathbf{B}\ \ln(\mathbf{s}(x,t))), \\ \mathbf{0} = \ln(\mathbf{K}^p) + \mathbf{E}\ \ln(\mathbf{c}(x,t)), \\ \mathbf{p} \geq \mathbf{0}. \end{cases} \tag{3}$$

The model is completed by mass balance equations applied to components. We define $\mathbf{T}$ and $\mathbf{W}$ as the vectors of total concentrations related to, respectively, aqueous and fixed components and denote by $\mathbf{C}$ and $\mathbf{F}$, respectively, the aqueous and fixed parts of the total concentrations of aqueous component $\mathbf{T}$. The mass balance equations are

$$\begin{cases} T_i(x,t) = C_i(x,t) + F_i(x,t), & i = 1, \ldots n_c, \\ C_i(x,t) = c_i(x,t) + \sum_{j=0}^{n_u} S_{ji} u_j(x,t), & i = 1, \ldots n_c, \\ F_i(x,t) = \sum_{j=0}^{n_v} A_{ji} v_j(x,t) + \sum_{j=0}^{n_p} E_{ji} p_j(x,t), & i = 1, \ldots n_c, \\ W_i(x,t) = s_i(x,t) + \sum_{j=0}^{n_v} B_{ji} v_j(x,t), & i = 1, \ldots n_s. \end{cases} \tag{4}$$

In a closed system, both $\mathbf{W}$ and $\mathbf{T}$ are given; in a reactive transport system, $\mathbf{W}$ is assumed to be constant, whereas $\mathbf{T}$ depends on the transport operator.

By combining Eqs. 3 and 4, we get a nonlinear system of $(n_c + n_s + n_p)$ equations, with $(n_c + n_s + n_p)$ unknowns $\ln(\mathbf{c})$, $\ln(\mathbf{s})$, $\mathbf{p}$. This system is completed by the constraint $\mathbf{p} \geq \mathbf{0}$ and can be written as

$$\begin{cases} \begin{pmatrix} \mathbf{T} - \mathscr{C}(\ln(\mathbf{c})) - \mathscr{F}(\ln(\mathbf{c}), \ln(\mathbf{s}), \mathbf{p}) \\ \mathbf{W} - \mathscr{W}(\ln(\mathbf{c}), \ln(\mathbf{s})) \\ \ln(\mathbf{K}^p) + E \ln(\mathbf{c}) \end{pmatrix} = \mathbf{0}, \\ \mathbf{p} \geq \mathbf{0}, \end{cases} \tag{5}$$

where $\mathscr{C}$, $\mathscr{F}$ and $\mathscr{W}$ express, respectively, $\mathbf{C}$, $\mathbf{F}$ and $\mathbf{W}$, as functions of the primary unknowns $\ln(\mathbf{c})$, $\ln(\mathbf{s})$ and $\mathbf{p}$. We assume that, for any $\mathbf{T}$, the system (Eq. 5) has a unique solution and that Newton's method converges locally towards this solution. This assumption is critical to obtain a well-posed mathematical model and to ensure convergence of the numerical model. We rewrite the chemical model as

$$\begin{cases} \Phi(\ln(\mathbf{c}), \ln(\mathbf{s}), \mathbf{p}, \mathbf{T}) = \mathbf{0}, \\ \mathbf{p} \geq \mathbf{0}. \end{cases} \tag{6}$$

If there is no precipitation–dissolution reaction, the model simplifies to

$$\Phi(\ln(\mathbf{c}), \ln(\mathbf{s}), \mathbf{T}) = \mathbf{0} \tag{7}$$

2.2 Transport equations

Now, we consider the transport of aqueous species by advection and dispersion. For a species c, the transport operator $\mathscr{L}(c, x)$ is given by:

$$\mathscr{L}(c,x) = \nabla.(\mathbf{a}(x).c - \mathbf{D}(x).\nabla(c)), \tag{8}$$

with $\mathbf{D}$ the effective diffusivity tensor and $\mathbf{a}$ the average velocity. We assume that these two parameters are independent of the species and of the time, but they may depend on space. Due to this assumption, we obtain a transport equation for each aqueous component, by using the total variables $\mathbf{T_i}$ and $\mathbf{C_i}$. For sake of simplicity, we consider no sink/source terms. Here, we use a TC formulation [18, 21], where $\mathbf{T}$ is the differential variable and where the operator L is applied to the variable $\mathbf{C}$. The mass conservation equations can be expressed for each total concentration T_i as

$$\varepsilon(x) \frac{\partial T_i}{\partial t}(x,t) + \mathscr{L}(C_i(x,t), x) = 0,\ i = 1, \ldots n_c, \tag{9}$$

where ε is the porosity of the medium, assumed to be independent of time but spatially variant. These partial differential equations are completed by boundary conditions and initial conditions.

2.3 Global system of partial differential algebraic equations (PDAE)

The global system couples chemistry equations with transport equations. The transport equations are written for each aqueous component, whereas the chemistry equations are expressed at each point of the

computational domain. We get a system of PDAEs, with $\mathbf{T}$, $\mathbf{C}$, $\ln(\mathbf{c})$, $\ln(\mathbf{s})$ and $\mathbf{p}$ as unknowns:

$$\begin{cases} \varepsilon \dfrac{\partial T_i}{\partial t} + \mathscr{L}(C_i, x) & = 0,\ i = 1, \ldots n_c, \\ \Phi(\ln(\mathbf{c}), \ln(\mathbf{s}), \mathbf{p}, \mathbf{T}) & = \mathbf{0}, \\ C_i - \mathscr{C}_i(\ln(\mathbf{c})) & = 0,\ i = 1, \ldots n_c, \\ \mathbf{p} & \geq 0, \\ +\text{initial conditions}, & \\ +\text{boundary conditions}. & \end{cases} \tag{10}$$

We assume that the system (Eq. 10) has a unique solution in a suitable function space. We also assume that it is possible to write the equations in weak form and to develop a rigorous mathematical framework.

3 Numerical model

We present now the global system, which couples chemistry and transport. In the method called direct substitution approach [13, 23], the variables C_i in the transport equations are replaced by the function $\mathscr{C}_i$. This approach strongly couples chemistry with transport. We therefore prefer to keep $\mathbf{C}$ as unknown and to add equations involving the functions $\mathscr{C}_i$.

In [11, 12], we describe in detail the numerical method we propose and we compare it with other methods. Here, we recall briefly the outline of our global approach. In order to solve the global system (Eq. 10), we use the method of lines [17]. This method is a general procedure for the solution of time-dependent partial differential equations involving the transformation of the partial differential equations into ordinary differential equations (ODE) or differential algebraic equations (DAEs). This method has a rigorous mathematical basis and can use efficient and robust DAE solvers for initial value ODE/DAEs. Let us assume that spatial discretisation is achieved by any classical Eulerian method such as the finite difference, the finite volume or the finite element methods. Let n_x be the number of cells (or more specifically, the number of degrees of freedom) in the mesh. Then, the discrete system can be written as

$$\begin{cases} \varepsilon \dfrac{d\mathbf{T}}{dt}(t) + \mathbf{L}_d * \mathbf{C}(t) + \mathbf{f} & = \mathbf{0}, \\ \Phi_d(\ln(\mathbf{c}(t)),\ \ln(\mathbf{s}(t)),\ \mathbf{p}(t), \mathbf{T}(t)) & = \mathbf{0}, \\ \mathbf{C}(t) - \mathscr{C}_d(\ln(\mathbf{c}(t))) & = \mathbf{0}, \\ \mathbf{T}(0) & = \mathbf{T}_{init}, \end{cases} \tag{11}$$

with $\mathbf{L}_d$ and $\mathbf{f}$ as the matrix and the vector obtained after spatial discretisation of the transport operator, respectively, Φ_d as the chemistry nonlinear system written at each discrete point, and the function $\mathscr{C}_d$ also written at each discrete point.

The system (Eq. 11) is a differential algebraic system (DAE) of index 1 [2, 12]. It contains $n_c n_x$ differential equations and $(2n_c + n_s + n_p)n_x$ algebraic equations. We assume that it has a unique solution in an suitable function space, and that the computed solution converges towards the solution of Eq. 10 when the cell size approaches zero. Again, this is a critical assumption in order to set up the numerical model in a mathematical framework. Let $\mathbf{Y} = (\mathbf{T}\ \mathbf{C}\ \ln(\mathbf{c}(t))\ \ln(\mathbf{s}(t))\ \mathbf{p}(t))$.

Global methods based on a direct substitution approach [13, 23] reduce the number of unknowns in the system by eliminating T and C and keeping only the chemistry unknowns $(\ln(\mathbf{c}(t))\ \ln(\mathbf{s}(t))\ \mathbf{p}(t))$. This substitution is generally done after time discretisation by an implicit first-order Euler scheme. In our method, we prefer to keep all the unknowns in order to use a general DAE solver. This approach reduces coupling at the price of a larger nonlinear system to solve. By classical transformations, the system (Eq. 11) can be written

$$\begin{cases} g(t, \mathbf{Y}(t), \dot{\mathbf{Y}}(t)) = \mathbf{0}, \\ \mathbf{Y}(t_0) = \mathbf{Y}_0, \\ \dot{\mathbf{Y}}(t_0) = \dot{\mathbf{Y}}_0. \end{cases} \tag{12}$$

where $\dot{\mathbf{Y}}$ denotes the time derivative of $\mathbf{Y}$.

In order to solve this system, we use a variable-order (from one to five), variable-coefficient, backward differentiation formula (BDF) in fixed-leading-coefficient form [1]. The BDF of order q is given by the multistep formula

$$\sum_{i=0}^{q} \alpha_{n,i} \mathbf{Y}_{n-i} = (t_n - t_{n-1}) \dot{\mathbf{Y}}_n, \tag{13}$$

where $\mathbf{Y}_n$ and $\dot{\mathbf{Y}}_n$ are approximations to $\mathbf{Y}(t_n)$ and $\dot{\mathbf{Y}}(t_n)$, respectively.

We define

$$G(\mathbf{Y}_n) = g\left(t_n, \mathbf{Y}_n, \frac{1}{(t_n - t_{n-1})} \sum_{i=0}^{q} \alpha_{n,i} \mathbf{Y}_{n-i}\right). \tag{14}$$

Then, each time step requires the solution of the system of nonlinear algebraic equations

$$G(\mathbf{Y}_n) = \mathbf{0}. \tag{15}$$

We solve this system by a modified Newton method [10, 24]. Each Newton iteration gives a linear system of equations of the form

$$\mathbf{J}\left[\mathbf{Y}_n^{k+1} - \mathbf{Y}_n^k\right] = -G\left(\mathbf{Y}_n^k\right), \tag{16}$$

where **J** is an approximation of the Jacobian of the function G. In order to save computational time, the Jacobian is kept unchanged during several Newton iterations and, possibly, several time steps, leading to a modified Newton method. The updating strategy for the Jacobian is embedded in the DAE solver [1].

The matrix **J**, of size $(3n_c + n_s + n_p)n_x$, where n_x is the number of discrete points, is sparse and nonsymmetric. We can reduce the size of the matrix down to $(n_c + n_s + n_p)n_x$, by using a substitution approach, keeping only the chemistry unknowns as in the DSA approach. In this paper, we keep all the unknowns and we solve the linear system (Eq. 16) by a direct nonsymmetric-pattern multifrontal method [8, 9]. Direct methods are quite efficient for solving systems with consecutive multiple right-hand sides, since the factorisation, which is the most time consuming part, is done only once.

We have implemented our method by using the IDA solver [14] from SUNDIALS [15], developed by the Lawrence Livermore National Laboratory. Linear solvers provided by IDA are a dense direct solver, a banded direct solver and a Krylov matrix-free iterative solver. We have interfaced a sparse direct multifrontal solver by adding a module based on UMFPACK [7].

We have implemented two methods for spatial discretisation [11]. In the first version, we use a cell-centered finite-volume method with a centered scheme for the diffusive flux and a first-order upwind approximation for the advective flux. This version is restricted to 1D domains with a fixed cell size. In the second version, we use a finite difference scheme with also an upwind approximation for advection, by interfacing the software MT3DMS [31]. Here, the cell size can be variable.

4 Results on the MoMas benchmark

We carried out several numerical experiments for validating our method [12]. We also did some numerical experiments with 2D domains [11]. Here, we consider numerical experiments using the MoMas benchmark [5] and present results for the so-called 1D easy test case, which is not so easy. This model is purely theoretical and is built in order to illustrate complexity of reactive transport models. The hydrodynamic model is simple with two media. The chemistry model is also simple with few species, and with only aqueous and sorption reactions. However, physical data are chosen in order to increase numerical difficulties. For example, hydrodynamic heterogeneities are quite large and reaction constants vary over several orders of magnitude. We present results for two sets of transport conditions, with the same velocity but with different diffusion tensors. These two test cases exhibit different kinds of difficulties.

4.1 Description of MoMas benchmark

Since this 1D easy test case of MoMas benchmark does not refer to a physical experiment, the units used are L for length, T for time and m for amount of substance. The computational domain is composed of two media: a dominant medium A and a medium B at the middle of the domain (Fig. 1). The medium B has a higher porosity ($\varepsilon = 0.5$ for medium B versus $\varepsilon = 0.25$ for medium A) and initially a higher reactivity ($W = 10\, m.L^{-3}$ for medium B versus $W = 1\, m.L^{-3}$ for medium A).

The geochemistry system is composed of four aqueous components and one fixed component, along with five secondary aqueous species and two secondary fixed species. Stoichiometric coefficients and equilibrium constants are given in Table 1. Mass action laws for each secondary species are read by rows and mass balance equations for each component are read by columns. For example, the mass action law for the species u_4 is given by

$$u_4 = K_4 \prod_{j=1}^{4} c_j^{S_{4,j}} = 0.1 \cdot (c_1)^0 \cdot (c_2)^{-4} \cdot (c_3)^1 \cdot (c_4)^3 m.L^{-3}. \tag{17}$$

Two different sets of transport parameters are applied in this domain, called advective and dispersive conditions. These two conditions have the same pore velocity value $a = 5.5 \times 10^{-3} L.T^{-1}$ but different dispersion values (Table 2).

Boundary conditions are defined by prescribed total concentrations at inflow boundary and prescribed zero concentration gradient at the outflow boundary. At the inflow boundary, prescribed concentrations vary in time: the injection period is the time interval [0 : 5,000] and the leaching period is the time interval

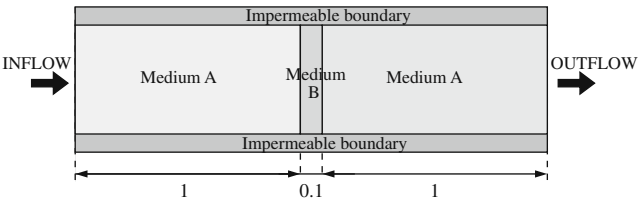

Fig. 1 Computational domain of the 1D easy test case of MoMas benchmark

Table 1 Stoichiometric coefficients and equilibrium constants for the 1D easy test case of MoMas benchmark

	c_1	c_2	c_3	c_4	s	K
u_1	0	−1	0	0	0	10^{-12}
u_2	0	1	1	1	0	1.0
u_3	0	−1	0	1	0	1.0
u_4	0	−4	1	3	0	0.1
u_5	0	4	3	1	0	10^{+35}
v_1	0	3	1	0	1	10^{+6}
v_2	0	−3	0	1	2	10^{-1}

[5,000 : 6,000]. Data are given in Table 3. Because we use logarithms in our model, concentrations cannot be equal to zero; therefore, initial and boundary values that are prescribed to zero are approximated by 10^{-20} in our implementation.

We present in Subsections 4.2 and 4.3 the figures suggested in the benchmark definition. More results can be found in [11]. Since we use an adaptive time step automatically chosen by the DAE solver, we do not run specific numerical experiments with a fixed time step and we do not study the behaviour when the time step approaches zero. On the other hand, we study the convergence behaviour when the cell size approaches zero. Since no reference solution is provided in the benchmark definition, we cannot easily define a convergence criterium. Thus, we choose to plot the concentrations for various cell sizes and to analyse the behaviour qualitatively. For all species and for both transport conditions, we observe convergence when we refine the mesh. However, we also observe some numerical artefacts such as oscillations and slower convergence in some specific zones of the time interval or the spatial domain. We choose to present these particular behaviours and try to give some explanation.

All the results presented are obtained with the first version of our software, using a finite volume method and a fixed cell size in the domain, except for some complementary results. The grey boxes represented in some of the figures enclose a particular zone where we have enlarged the plot in order to provide some additional information.

In all computations, for both advective and dispersive test cases and for all mesh sizes, we use the same tolerances in the DAE solver: ATOL $= 10^{-12}$ and RTOL $= 10^{-9}$. We did not try to reduce computational time by using larger thresholds because we aimed at obtaining accurate results.

Table 2 Values of the dispersion coefficient D $(L^2.T^{-1})$ as functions of the medium and of the transport conditions for the 1D easy test case of MoMas benchmark

	Medium A	Medium B
Advective case	5.5×10^{-5}	3.3×10^{-4}
Dispersive case	5.5×10^{-2}	3.3×10^{-1}

Table 3 Boundary and initial conditions for the 1D easy test case of MoMas benchmark

	c_1	c_2	c_3	c_4	s
Initial values of the total concentrations (m L^{-3})					
Medium A	0.0	−2.0	0.0	2.0	1.0
Medium B	0.0	−2.0	0.0	2.0	10.0
Prescribed total concentrations at the inflow boundary (m L^{-3})					
Injection t ∈ [0; 5000] (T.)	0.3	0.3	0.3	0.0	
Leaching t ∈ [5000; 6000] (T.)	0.0	−2.0	0.0	2.0	

4.2 Results for the advective test case

We carried out simulations with a varying number of cells in order to check convergence ($n_x = 50$, 100, 200, 400, 800, 1,600, 2,100, 3,200). We observe a global convergence and observe that the sharp fronts are well captured when we refine the mesh. Our results are in good agreement with those of other participants in this MoMas benchmark [4, 16, 19, 22]. Because we want to illustrate that our global approach is able to solve difficult numerical problems with high accuracy, we choose to present the results obtained with a fine mesh ($n_x = 1{,}600$ cells). Figures 2, 3, 4, 5, 6, 7, 8, 9, 10, 11 and 12 show the results obtained for the advective condition. Figures 2–7 plot the evolution of some species at a given point in function of time, whereas Figs. 8–12 show the evolution of some species at a given

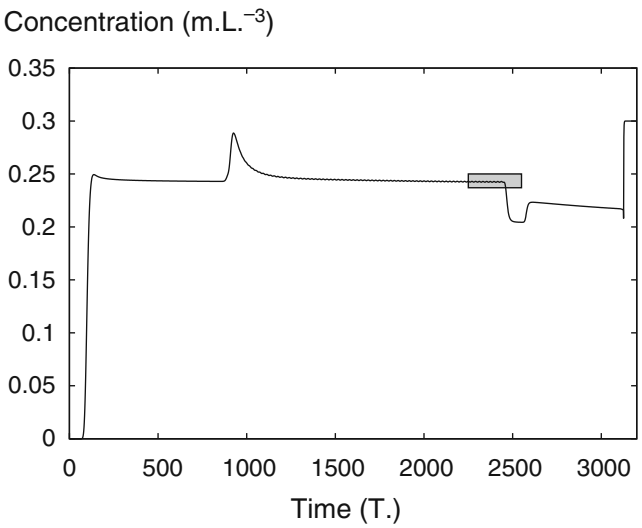

Fig. 2 Elution curve of total dissolved concentration C_3 at $x = 2.1L$ for the advective 1D easy test case with $n_x = 1{,}600$ cells

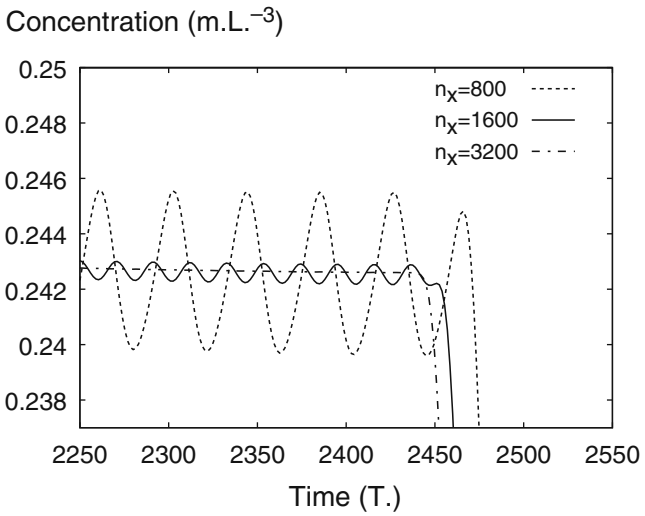

Fig. 3 Elution curve of total dissolved concentration C_3 at $x = 2.1L$ for the advective 1D easy test case: from Fig. 2, zoom on oscillations with three spatial grids

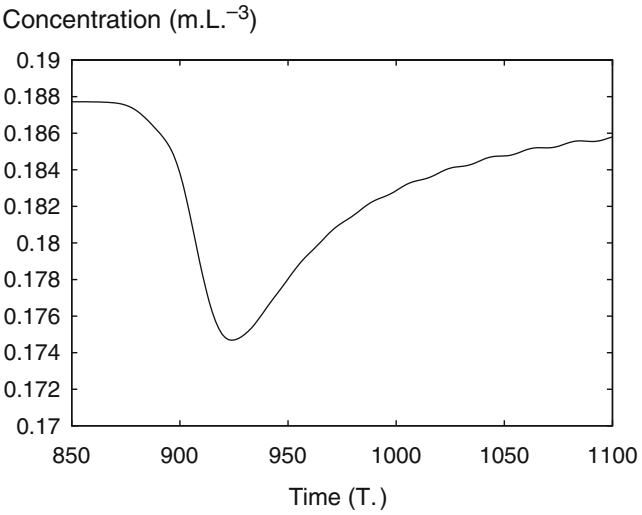

Fig. 5 Elution curve of component c_3 at $x = 2.1L$ for the advective 1D easy test case with $n_x = 1{,}600$ cells

time in function of space. In order to illustrate some numerical difficulties, we show zooms with a coarser mesh ($n_x = 800$) and a finer mesh ($n_x = 3{,}200$).

We first comment on results at the outflow point. Regarding the elution curve for the total aqueous component C_3 at $x = 2.1L$, we focus on the time period [2,250 : 2,500] as shown by the grey box in Fig. 2. This time interval is chosen to illustrate the oscillatory behaviour of the curve. We plot the concentration for three spatial grids in Fig. 3 and observe oscillations for the two coarser grids. However, when the mesh is refined, the amplitude of the oscillations decreases and the frequency increases so that no oscillation is visible with the finest grid.

We also used the second version of our software, with a finite difference method and a variable cell size. In Fig. 4, we plot the same concentration for two different spatial grids, with a coarse mesh and a fixed cell size and with a mesh refined around medium B. Both grids have $n_x = 420$ cells. We observe that oscillations disappear for the mesh refined around medium B.

Therefore, we conclude that these oscillations are due to the numerical scheme. Also, we conclude that

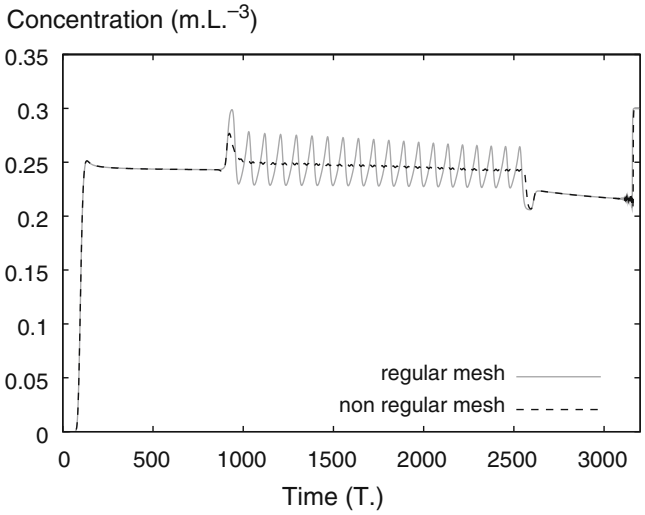

Fig. 4 Elution curve of total dissolved concentration C_3 at $x = 2.1L$ for the advective 1D easy test case. Results with a coarse grid with a fixed cell size and with a grid locally refined around medium B. Both grids use $nx = 420$ cells

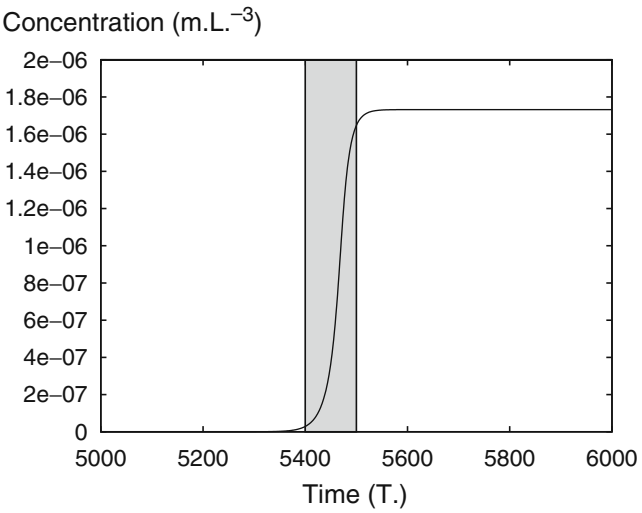

Fig. 6 Elution curve of species u_1 at $x = 2.1L$ for the advective 1D easy test case with $n_x = 1{,}600$ cells

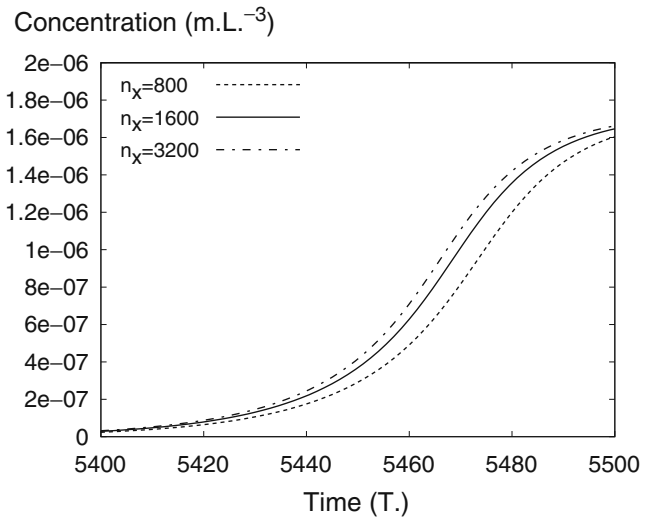

Fig. 7 Elution curve of species u_1 at $x = 2.1L$ for the 1D advective easy test case: from Fig. 6, zoom with three spatial grids

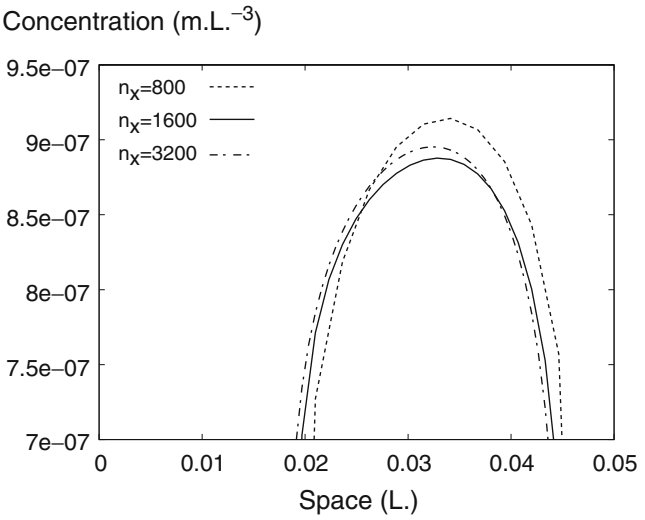

Fig. 9 Concentration profile for the advective 1D easy test case of species u_1 at $t = 10.T.$: from Fig. 8, zoom on peak for three spatial grids

local refinement is a cheap way to remove these oscillations.

Oscillations are also observed for the elution curve of the aqueous component c_3 at the outflow point. They are still visible in Fig. 5 because the time scale of the figure is refined here. However, they disappear when we refine the mesh.

Concerning the elution curve for the aqueous secondary species u_1 at $x = 2.1L$, no oscillation is visible (Fig. 6) and the sharp front is quite accurate. However, convergence is slower near this sharp front than in other areas. When we focus on the time interval [5,400 : 5,500] in Fig. 7, we observe some differences between the three spatial grids, which are larger than in other areas.

Therefore, we observe that both the finite volume and the finite difference methods converge experimentally when the cell size approaches zero. However, locally, at some point or at some time, the distance between two curves (for two cell sizes) may not decrease in a monotone way. The behaviour is improved by local refinement; thus, some a posteriori error estimation could be very useful for this test case.

After these comments on the concentrations at the outflow point, we analyse the results at a given time.

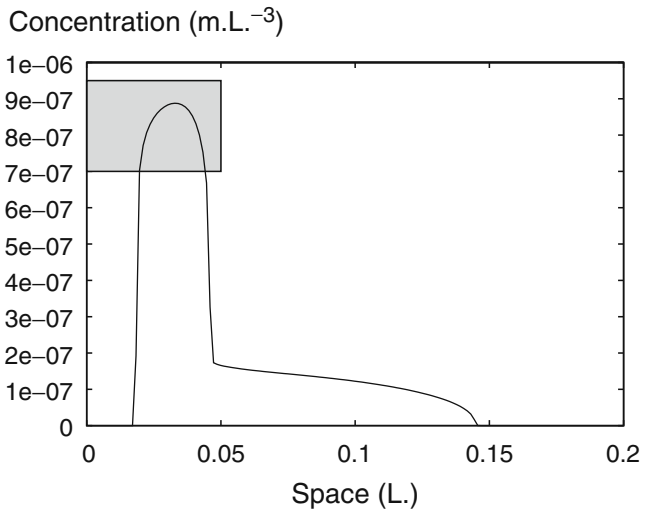

Fig. 8 Concentration profile for the advective 1D easy test case of species u_1 at $t = 10.T$ with $n_x = 1{,}600$ cells

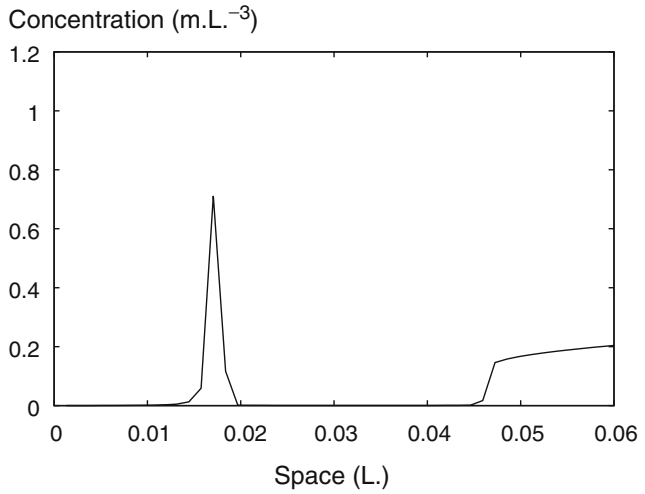

Fig. 10 Concentration profile for the advective 1D easy test case of fixed component s at $t = 10.T.$ with $n_x = 1{,}600$ cells

Regarding the concentration profile of the aqueous secondary species u_1 at $t = 10T$, in Fig. 8, we observe a high peak between $x = 0.015L$ and $x = 0.05L$; since convergence is slower in this area, Fig. 9 shows a zoom of the peak with the three spatial grids. We observe that the peak becomes more accurate when we refine the mesh.

Figure 10 shows the concentration profile for the sorbed component s at the beginning of the injection period, for $t = 10T$, near the left boundary of the domain. In the benchmark definition, it is required to plot the result in the space interval [0 : 0.06], which is quite small; therefore, we show results with only a fine mesh with $n_x = 1{,}600$ cells, in order to use 45 cells in the space interval. With a coarser mesh, the concentration peak observed is not so sharp.

Finally, the concentration profile of aqueous secondary species u_2 at time $t = 5{,}010T$ is shown in Fig. 11. Here too, we still observe convergence when we enlarge the critical zone (Fig. 12).

We now discuss computational requirements of our global method for this test case. Computations are done on an Intel Pentium 4 with a frequency of 3 GHz, a memory RAM of 1 Gb and a memory cache of 1 Mb, under the operating system Linux Fedora Core 6. We use a unit time based on the CPU time required for a BLAS3 operation. More specifically, this operation is the product of two (1,000 × 1,000) real matrices. We make this computation twice, either with the BLAS function from the ATLAS implementation of BLAS library or with three classical loops of computation. Both units are called, respectively, U_{blas} and $U_{\text{no blas}}$. For the sake of information, we get $U_{\text{blas}} = 0.43$ s and $U_{\text{no blas}} = 8.5$ s.

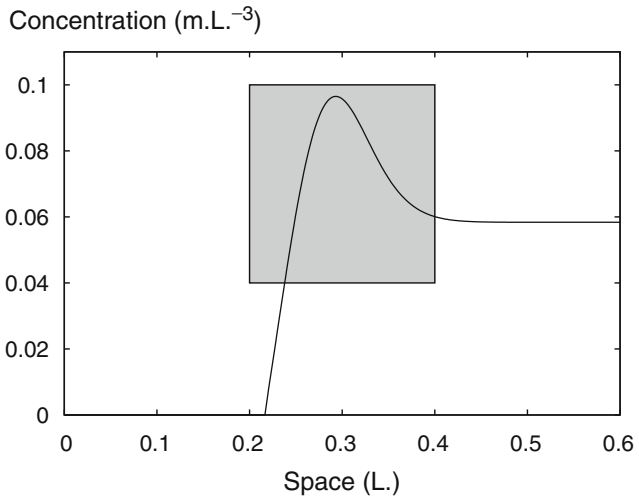

Fig. 11 Concentration profile of species u_2 at $t = 5{,}010.T$ for the 1D advective easy test case with $n_x = 1{,}600$ cells

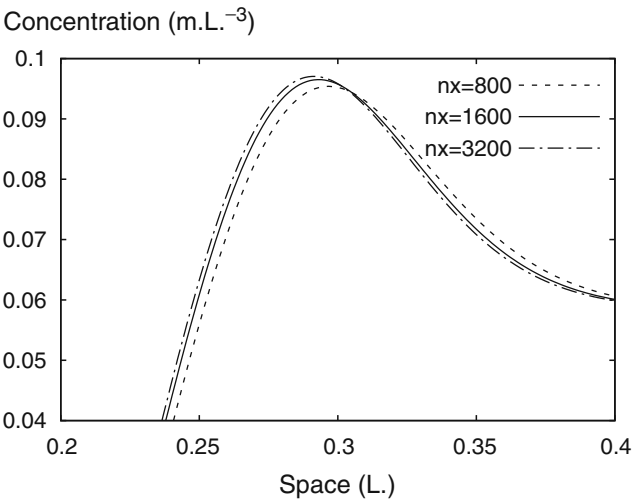

Fig. 12 Concentration profile for the 1D advective easy test case of species u_2 at $t = 5{,}010.T$.: from Fig. 11, zoom on the peak with three spatial grids

The BLAS library is optimised to perform basic linear algebra operations. In our software, only the sparse linear solver uses BLAS3 operations, so that the effective computational time unit is in between U_{blas} and $U_{\text{no blas}}$.

In Table 4, we give the computing times expressed in these two units for a varying mesh size. Results are given here for the first version with a fixed cell size in the domain. We observe a complexity of about $O(n_x^{1.8})$. Two effects induce this nonlinear complexity: the factorisation of the matrix follows a power law, and the number of time steps increases when we refine the mesh. We could adapt the various parameters of the DAE solver and refine only locally the mesh in order to reduce the CPU time.

4.3 Results for the dispersive test case

As for the advective test case, we carried out simulations with a varying number of cells ($n_x = 42$, 84, 168, 336, 672, 1,344). Here too, we use the first version of the method with a finite volume method and a fixed

Table 4 CPU time obtained for different mesh sizes for the advective test case in units of time with BLAS function (U_{blas}) and in units of time without BLAS function ($U_{\text{no blas}}$)

Mesh size n_x	CPU time (in U_{blas})	CPU time (in $U_{\text{no blas}}$)
50	698	35
100	2,511	127
200	8,537	432
400	29,929	1,514
800	111,565	5,644
1,600	379,080	19,177
3,200	1,358,701	68,734

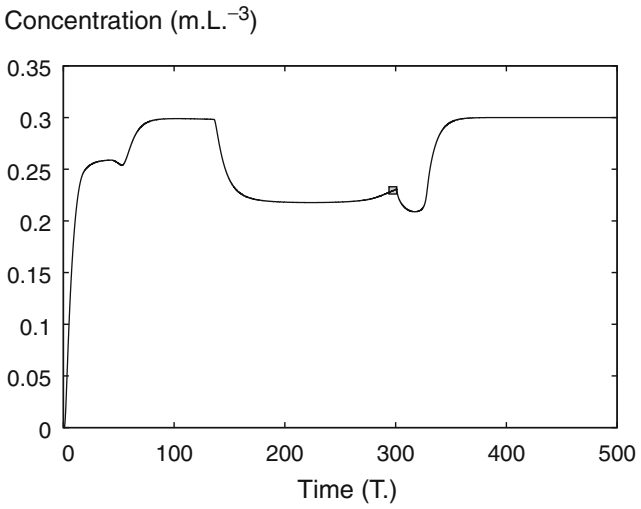

Fig. 13 Elution curve of total dissolved concentration C_3 at $x = 2.1L$ for the dispersive 1D easy test case with $n_x = 672$ cells

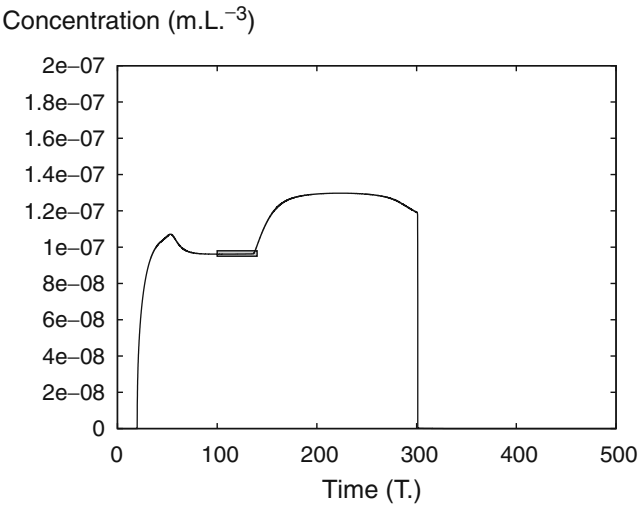

Fig. 15 Elution curve of species u_1 at $x = 2.1L$ for the dispersive 1D easy test case with $n_x = 672$ cells

cell size. We also obtain a global convergence and observe that the sharp fronts are well captured when we refine the mesh. As for the advective test case, we choose to present the results obtained with a fine mesh ($n_x = 672$ cells). The method gives accurate results with a coarser mesh than for the advective condition.

Figures 13, 14, 15, 16, 17, 18, 19, 20, 21 and 22 show the different results obtained concerning the dispersive 1D easy test case. Figures 13–19 present the evolution of some species in function of time, whereas Figs. 20–22 show the evolution of some species in function of space. For this test case also, we present simulation results with a coarser mesh ($n_x = 336$) and a finer mesh ($n_x = 1{,}344$), in order to illustrate some numerical difficulties.

We first comment on results at the outflow point. Concerning the elution curve for the total dissolved concentration C_3 at $x = 2.1L$, we focus on time period $[280 : 310]$ as shown by the grey box in Fig. 13 in order to underline numerical difficulties. Oscillations are indeed visible in Fig. 14. As for the advective test case, the amplitude of the oscillations decreases and the frequency of the oscillations increases when we refine the mesh. However, the oscillations seem to be less important than for the advective test case (Fig. 3).

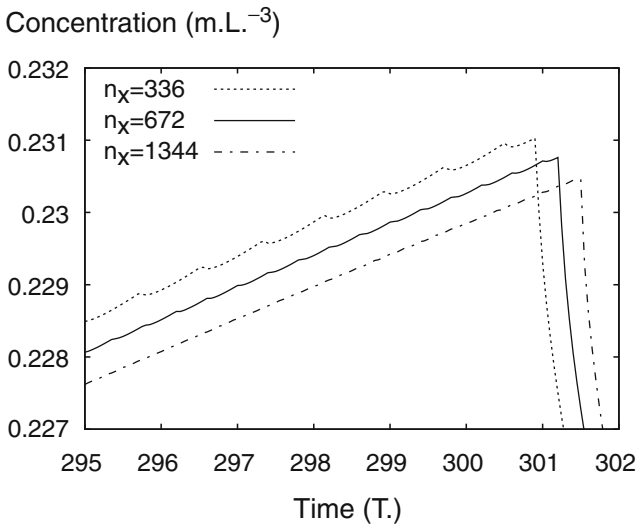

Fig. 14 Elution curve of total dissolved concentration C_3 at $x = 2.1L$ for the dispersive 1D easy test case: from Fig. 13, zoom on oscillations with three spatial grids

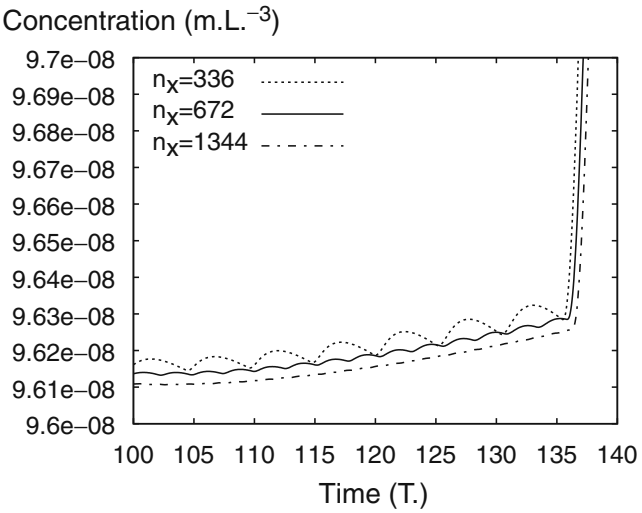

Fig. 16 Elution curve of species u_1 at $x = 2.1L$ for the dispersive 1D easy test case: from Fig. 15, zoom on oscillations with three spatial grids

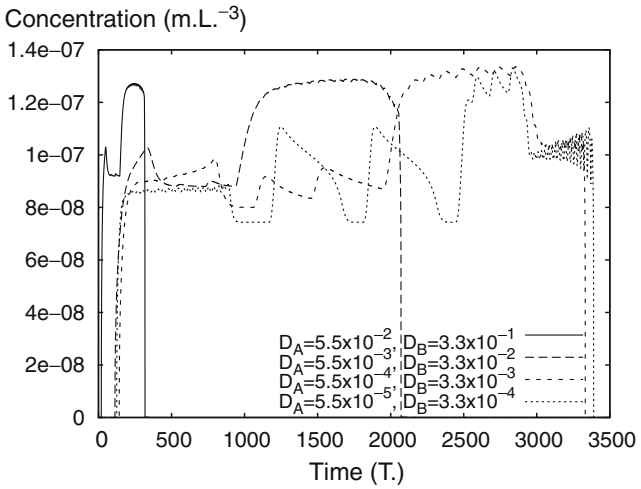

Fig. 17 Elution curve of species u_1 at $x = 2.1L$ for the 1D easy test case with varying dispersion conditions and with $n_x = 50$ cells

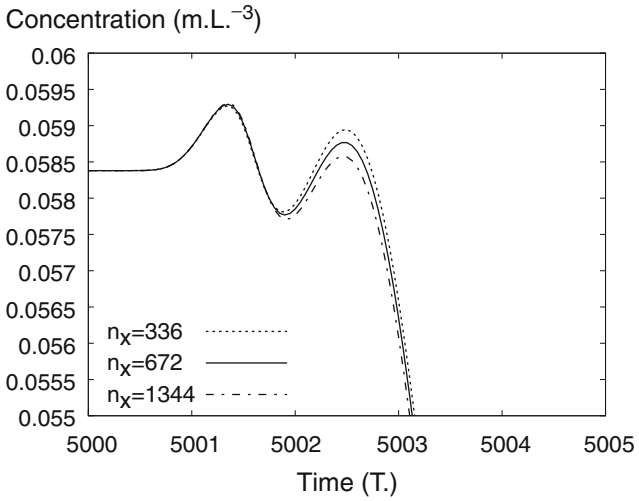

Fig. 19 Elution curve of species u_2 at $x = 2.1L$ for the dispersive 1D easy test case: from Fig. 18, zoom on two peaks for three spatial grids

We observe a similar behaviour for the elution curve of the species u_1; when we enlarge the area plotted in Fig. 15, corresponding to the time interval [100 : 140], we observe oscillations (Fig. 16) which are no longer visible for the finest mesh. Here too, oscillations are not as important as in the advection test case.

In order to analyse this numerical artefact, we run other test cases with the same chemistry but with transport conditions where diffusion coefficients increase from the advective condition to the dispersive condition (Fig. 17). Although we still observe some oscillations in the dispersive case, their amplitude clearly increases when the diffusion coefficients decrease. We suspect that the first-order upwind scheme used for advection induces numerical dispersion. This artefact has a reduced impact if the model includes physical dispersion.

Regarding the species u_2, we enlarge the area plotted in Fig. 18, corresponding to two peaks of concentration. In this time interval, we observe a slower convergence than in the whole time interval, but no numerical oscillations (Fig. 19).

For all the species, we observe convergence when we refine the mesh. A fine mesh is necessary at some point or at some time in order to reduce oscillations or to improve accuracy. Adaptive mesh refinement based

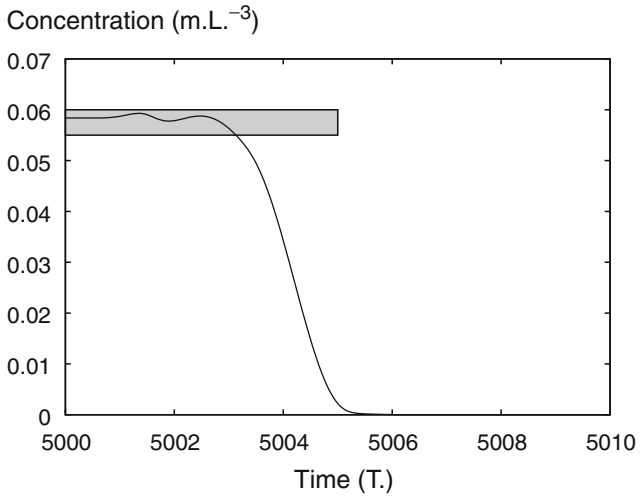

Fig. 18 Elution curve of species u_2 at $x = 2.1L$ for the dispersive 1D easy test case for $n_x = 672$ cells

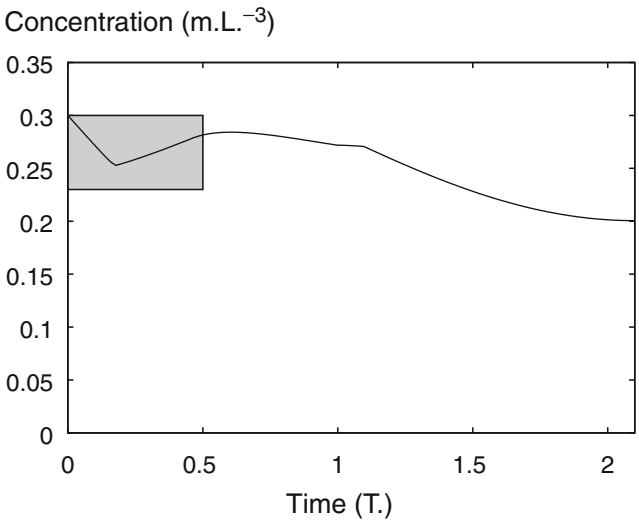

Fig. 20 Concentration profile of total dissolved concentration C_2 at $t = 10.T$ for the dispersive 1D easy test case with $n_x = 672$ cells

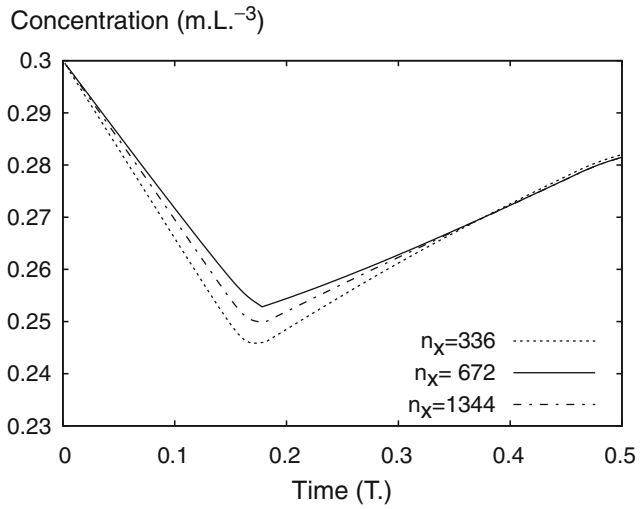

Fig. 21 Concentration profile of total dissolved concentration C_2 at $t = 10.T$ for the dispersive 1D easy test case: from Fig. 20, zoom on the local minimum for three spatial grids

on a posteriori error estimation could be very useful in order to reduce computational cost and to preserve accuracy.

After these comments on the data expressed as functions of time, we comment on the data expressed as functions of space. In Fig. 20, we plot the concentration profile of the total dissolved concentration C_2 and we enlarge the grey area in Fig. 21, corresponding to the spatial interval $[0 : 0.5]$. We choose this zone because convergence is slower here. Locally, the distance between two curves does not decrease regularly when we refine the mesh. Some error estimation could be

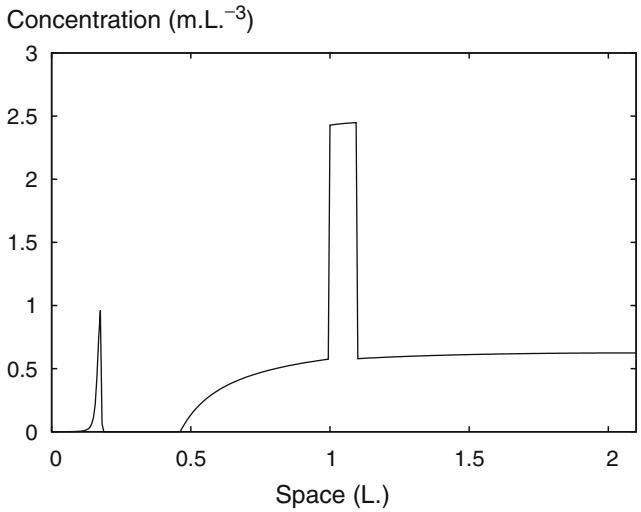

Fig. 22 Concentration profile for dispersive easy test case 1D for concentration of fixed component s at $t = 10.T$. for $n_x = 672$ cells

Table 5 CPU time obtained for different mesh sizes for the dispersive test case in time units with BLAS function (U_{blas}) and in time units without BLAS function ($U_{\text{no blas}}$)

Mesh size	CPU time (in U_{blas})	CPU time (in $U_{\text{no blas}}$)
42	1,403	71
84	2,582	131
168	10,772	545
336	32,340	1,636
672	122,416	6,193
1,344	672,350	34,013

useful here to analyse in more detail the convergence behaviour.

Finally, results for the fixed component s are shown in Fig. 22. Here, the first peak in the space domain $[0; 0.25]$ is not correctly captured if the mesh is too coarse.

Now, we discuss computational requirements for this dispersive test case. The CPU times obtained for different mesh sizes are given in Table 5 with the same units as for the advective test case.

The observed CPU complexity is about in $O({n_x}^{2.4})$, with a higher exponent than in the advective case. We must further analyse this computational complexity. In particular, we must analyse the frequency of Jacobian updates.

4.4 Discussion

We have presented results as suggested in the benchmark definition. They are in good agreement with those of other participants in the benchmark study [4, 16, 19, 22].

In both advective and dispersive test cases, we observe convergence of the concentrations when we refine the mesh. However, locally, around some sharp fronts, for example, convergence is slower than in other areas and the distance between the values does not seem to decrease in a monotone way. Also, for the two transport conditions, we observe oscillations in the concentrations of some chemical species. Since a refinement of the mesh clearly reduces these oscillations, we can assume that they are related to the numerical scheme. Moreover, these oscillations are more important for advection-dominated test cases. We suspect that the first-order upwind advection scheme induces numerical dispersion. The reactive transport model is not a classical advection–diffusion equation because of the coupling with chemistry. Here, it is nonlinear and couples the time derivative $\frac{\partial T}{\partial t}$ with the transport operator $\mathscr{L}(C)$ through the chemistry algebraic equations. Thus, the classical properties of the first-order upwind scheme for advection and the centered

scheme for diffusion are probably no longer true. In particular, it seems that the global method is not a TVD scheme.

For the same number of cells, the dispersive test case requires more CPU time than the advective test case. On the other hand, a coarse mesh yields enough accuracy in the dispersive case. We need to further analyse the computational complexity. Also, we plan to reduce the size of the linear systems by substitution in order to reduce the cost of the direct sparse linear solver. We choose to present accurate results where most of the oscillations are removed. Therefore, we use a sufficiently refined mesh and sufficiently small tolerances in the DAE solver. As a result, CPU requirements are quite high for these 1D test cases. In order to reduce CPU time, we have developed a second version where it is possible to locally refine the mesh. Preliminary results where we refine locally around medium B are quite satisfactory. We get accurate results with a smaller number of cells, thus, with a reduced CPU time. Adaptive mesh refinement would be very useful for these test cases.

5 Conclusion

In this paper, a global method based on a method of lines and a system of DAE has been defined and used for reactive transport problems. In a first step, spatial discretisation leads to a discrete system of DAE. In a second step, implicit time discretisation is applied. At each time step, nonlinear equations are solved by a modified Newton-LU method. The DAE solver includes an adaptive time step and a strategy to update the Jacobian only when necessary.

Our global method is applied on the 1D easy test case proposed in the MoMas benchmark. This test case is representative of the difficulties arising in reactive transport simulations: strongly nonlinear systems with sharp fronts and stiff reactions. We experimentally checked convergence of numerical results by refining the mesh. For both transport conditions defined in the benchmark, we observe oscillations. Since they are damped by refining the mesh, we assume that these oscillations are due to numerical dispersion. Indeed, it is not clear whether the coupled numerical scheme is monotone.

We present results with high CPU requirements because our tolerance thresholds in the DAE solver are very small and because we use a fine mesh in order to get accurate results. We could already reduce the time by refining the mesh only locally, without loosing too much accuracy. We plan to further cut down the time by applying a substitution approach at the linear level, which reduces the matrix size.

Currently, our method has been applied to specific geochemistry systems. We reckon that it is not difficult to introduce kinetic reactions and activity coefficients. It is harder to deal with minerals, since the nonlinear system becomes non-differentiable. We plan to use semismooth Newton methods for solving these problems.

References

1. Brenan, K., Campbell, S., Petzold, L.: Numerical Solution of Initial-Value Problems in Differential-Algebraic Equations. North-Holland, Amsterdam (1996)
2. Brown, P.N., Hindmarsh, A.C., Petzold, L.R.: Consistent initial condition calculation for differential-algebraic systems. SIAM J. Sci. Comput. **19**(5), 1495–1512 (1998)
3. Carrayrou, J., Mose, R., Behra, P.: Operator-splitting procedures for reactive transport and comparison of mass balance errors. J. Contam. Hydrol. **68**, 239–268 (2004)
4. Carrayrou, J.: Looking for some reference solutions for the Reactive Transport Benchmark of MoMaS with SPECY. Comput. Geosci. (2009). doi:10.1007/s10596-009-9161-y
5. Carrayrou, J., Kern, M., Knabner, P.: Reactive transport benchmark of MoMaS. Comput. Geosci. (2009). doi:10.1007/s10596-009-9157-7
6. Cirpka, O., Helmig, R.: Comparison of approaches for the coupling of chemistry to transport in groundwater systems. Notes Numer. Fluid Dyn. **59**, 102–120 (1997)
7. Davis, T.A.: UMFPACK Version 5.0 User Guide. Department of Computer and Information Science and Engineering, University of Florida, Gainesville (2006)
8. Davis, T.A., Duff, I.S.: An unsymmetric-pattern multifrontal method for sparse lu factorization. SIAM J. Matrix Anal. Appl. **18**(1), 140–158 (1997)
9. Davis, T.A., Duff, I.S.: A combined unifrontal/multifrontal method for unsymmetric sparse matrices. ACM Trans. Math. Softw. **25**(1), 1–20 (1999)
10. Dennis, J.E., Schnabel, R.B.: Numerical Methods for Unconstrained Optimization and Nonlinear Equations. Series in Comput. Math. Prentice Hall, Englewood Cliffs (1983)
11. de Dieuleveult, C.: An efficient and robust global method for reactive transport. Ph.D. thesis, University of Rennes 1 (2008)
12. de Dieuleveult, C., Erhel, J., Kern, M.: A global strategy for solving reactive transport equations. J. Comput. Phys. **228**, 6395–6410 (2009)
13. Hammond, G., Valocchi, A., Lichtner, P.: Application of Jacobian-free Newton-Krylov with physics-based preconditioning to biogeochemical transport. Adv. Water Resour. **28**, 359–376 (2005)
14. Hindmarsh, A.C., Brown, P.N., Grant, K.E., Lee, S.L., Serban, R., Shumaker, D.E., Woodward, C.S.: Sundials: suite of nonlinear and differential/algebraic equation solvers. ACM Trans. Math. Softw. **31**(3), 363–396 (2005)
15. Hindmarsh, A.C., Serban, R.: User Documentation for IDA v2.3.0. Center for Applied Scientific Computing, Lawrence Livermore National Laboratory (2005)
16. Hoffmann, J., Kräutle, S., Knabner, P.: A parallel global-implicit 2-D solver for reactive transport problems in porous

media based on a reduction scheme and its application to the MoMaS benchmark problem. Comput. Geosci. (2009, in press)
17. Kanney, J.F., Miller, C.T., Barry, D.: Comparison of fully coupled approaches for approximating nonlinear transport and reaction problems. Adv. Water Resour. **26**, 353–372 (2003)
18. Krikner, D., Reeves, H.: Multicomponent mass transport with homogeneous and heterogeneous chemical reactions: effect of the chemistry on the choice of numerical algorithm 1. theory. Water Resour. Res. **24**, 1719–1729 (1988)
19. Lagneau, V., van der Lee, J.: HYTEC results of the MoMas reactive transport benchmark. Comput. Geosci. (2009). doi:10.1007/s10596-009-9159-5
20. van der Lee, J., De Windt, L.: Present state and future directions of modeling of geochemistry in hydrogeological systems. J. Contam. Hydrol. **47**, 265–282 (2001)
21. Lucille, P., Burnol, A., Ollar, P.: Chemtrap: a hydrogeochemical model for reactive transport in porous media. Hydrol. Process. **14**, 2261–2277 (2000)
22. Mayer, K.U., MacQuarrie, K.T.B.: Solution of the MoMaS reactive transport benchmark with MIN3P — model formulation and simulation results. Comput. Geosci. (2009). doi:10.1007/s10596-009-9158-6
23. Molins, S., Carrera, J., Ayora, C., Saaltink, M.W.: A formulation for decoupling components in reactive transport problems. Water Resour. Res. **40**, W10,301 (2004)
24. Ortega, J., Rheinboldt, W.: Iterative Solution of Nonlinear Equations in Several Variables. Comput. Sci. Appl. Math. Academic, London (1970)
25. Saaltink, M.W., Carrera, J., Ayora, C.: On the behavior of approaches to simulate reactive transport. J. Contam. Hydrol. **48**(3), 213–235 (2001)
26. Steefel, C.I., MacQuarrie, K.T.: Approaches to modeling of reactive transport in porous media. In: Lichtner, P., Steefel, C., Oelkers, E. (eds.) Reactive Transport in Porous Media, *Rev. Mineral.*, vol. 34, pp. 83–125. Mineral. Soc. Am. (1996)
27. Valocchi, A., Street, R., Roberts, P.: Transport of ion-exchanging solutes in groundwater: chromatographic theory and field simulation. Water Resour. Res. **17**(5), 1517–1527 (1981)
28. Walter, A., Frind, E., Blowes, D., Ptacek, C., Molson, J.: Modeling of multicomponent reactive transport in groundwater 1. Model development and evaluation. Water Resour. Res. **30**(11), 3137–3148 (1994)
29. Yeh, G.T., Tripathi, V.S.: A critical evaluation of recent developments in hydrogeochemical transport models of reactive multichemical components. Water Resour. Res. **25**(1), 93–108 (1989)
30. Yeh, G.T., Tripathi, V.S.: A model for simulating transport of reactive multispecies components: model development and demonstration. Water Resour. Res. **27**(12), 3075–3094 (1991)
31. Zheng, C., Wang, P.P.: MT3DMS—A Modular Three-Dimensional Multispecies Transport Model for Simulation of Advection, Dispersion and Chemical Reactions of Contaminants in Groundwater Systems. SS Papadopulos, Bethesda (1999)
32. Zysset, A., Stauffer, F., Dracos, T.: Modeling of chemically reactive groundwater transport. Water Resour. Res. **30**(7), 2217–2228 (1994)